

On-line energy discrimination at DAQ front-end level on pixelated TOF-PET systems

Carlos Zorraquino^{a,b,*}, Luis Ferramacho^c, Ricardo Bugalho^c, Milan Zvolsky^d, Agostino Di Francesco^e, Carlos Leong^c, Tahereh Niknejad^e, Jose C. Silva^{e,c}, Rui Silva^e, Miguel Silveira^c, Stefaan Tavernier^{c,f}, Pedro Guerra^{a,b}, Joao Varela^{e,c}, Andres Santos^{a,b}

^aBiomedical Image Technologies Lab, Universidad Politécnica de Madrid, Av. Complutense 30, 28040 Madrid, Spain

^bCIBER-BBN - Centro de Investigación Biomédica en Red en Bioingeniería, Biomateriales y Nanomedicina, Av. Monforte de Lemos, 3-5. Pabellón 11. Planta 0 28029 Madrid

^cPETsys Electronics, Taguspark, Edificio Tecnología I, 26, 2740-122 Oeiras, Portugal

^dInstitute of medical engineering, university of Lübeck, Lübeck, Germany

^eLIP - Laboratório de Instrumentação e Física Experimental de Partículas, Av. Elias Garcia 14-1, 1000-149 Lisboa, Portugal

^fVrije Universiteit Brussel, Brussel, Belgium

Abstract

Pixelated PET systems produce higher count rates as they integrate several detecting channels per detector module. An increased data flow from the detectors poses higher needs on the bandwidth requirements. We aim to optimize the bandwidth usage efficiency by filtering on the fly the detected events with non valid energies. PET systems with a SiPM-ASIC readout scheme are being extensively used to get enhanced images on Time-Of-Flight PET scanners. These kind of digital readout systems are specially interesting for the application of on-line processing techniques given the ease of access to each detected event digital information. This study pursues the analysis of on-line processing techniques on the DAQ front-end level (on-detector electronics) for pixelated PET systems with SiPM-ASIC readout. In particular, we worked with a tunable on-line energy discriminating stage. For the optimization of its hardwired internal limits we analyzed the system energy space. We explored different solutions dependent or not on the system's energy calibration. Results obtained through the different filter versions confirm the minimal resources consumption of such processing techniques implemented at DAQ front-end level. Our experiences showed how the filtering process reduces the bandwidth needs excluding from the data stream all non valid energy events and thus improving the system sensitivity under saturation conditions. Additionally, these experiments highlight how setting proper energy limits we ensure the preservation of the system performance, which maintains its original energy and time resolution. Under the light of these findings, we see a great potential on the application of on-line processing techniques for Time-Of-Flight PET at the DAQ front-end level (on-detector electronics) and so we envisaged more complex processing methods.

Keywords: PET, TOF-PET, Pixelated PET, SiPM, ASIC, DAQ, Digital readout, On-line processing

1. Introduction

State of the Art in Positron Emission Tomography (PET) scanners shows a tendency towards pixelated detectors opposed to monolithic ones. Pixelated systems achieve better spatial and time resolutions than traditional block detectors[1]. In re-

turn, the use of highly pixelated scanners integrating thousands of detecting channels implies a higher degree of complexity on the system. The higher the degree of pixelation in the detector the more readout channels are required, thus increasing the cost and complexity of the data acquisition (DAQ)[2] which would deal with higher system count rates. And an uncontrolled aggregated data flow from thousands of detecting channels could saturate the system. Traditionally, the workstation collecting all the events produced by the system performs

*Corresponding author

Email address: carlos.zorraquino@upm.es (Carlos Zorraquino)

an off-line event energy discrimination. This solution reduces the data processing computational costs cutting down the volume of data to analyze. Nevertheless, applying this technique on a highly pixelated and high count rate system does not ease the congestion issue. On these cases the volume of data transferred from the detector electronics to the acquisition workstation tends to saturate the link between detector and data collector. Applying no particular policy to discriminate and discard events, the system drops under saturation any event regardless of the information it contains, which results in a decrement of the system sensitivity. New on-line techniques are appearing on literature to cope with this situation. On-line energy discrimination applied for the rejection of the events whose energy lays outside the valid PET energy window is one of these techniques. It can reduce the volume of data transferred without negative implications in the system performance[3][4].

Given its system characteristics, the EndoTOFPET-US scanner[5][6] could take advantage from the application of these procedures. The EndoTOFPET-US is an asymmetric PET scanner whose bigger detector contains 4096 detecting channels composed by a Lutetium-Yttrium Oxyorthosilicate (LYSO) crystal pixel coupled to a Silicon Photo-Multiplier (SiPM) channel. Simulations tell us that this 4K channels detector produces a count rate of 40MHz[7], while real acquisitions show that the practical bandwidth (BW) limit on the system goes down to 25MHz. Given the small size of the opposite detector, which produces no more than 200KHz, when the system works in coincidence mode the data rate will be below the saturation point. However, when operating the system in singles mode for detectors calibration, the bigger detector will saturate the system. Hence, the DAQ of this system[8][9] would benefit from the on-line discrimination of events. It would optimize the usage of the available BW limiting the transmission to the useful data. Thus we propose an on-line discriminating solution to be implemented on the on-detector electronics, which aims to control the data volume produced by each detector module while minimizing its impact on system sensitivity and performance. Such on-detector and on the fly filtering process would be greatly useful for highly pixelated PET scanners like the EndoTOFPET-US. It would improve detector Signal to Noise Ratio (SNR) reducing the system BW requirements.

The ultimate goal of this work is to analyze the benefits and costs of applying on-line processing techniques on the DAQ of cutting-edge PET systems making use of SiPMs readout by Application Specific Integrated Circuits (ASIC). PET detectors read by ASICs are specially adequate for the application of these on-line filtering techniques given the accessibility to the event data preprocessed and digitized by the ASICs at the DAQ front-end level on the on-detector electronics. At the DAQ front-end level of SiPM-ASIC systems we have available the digital event information generated by the ASIC upon detection of a SiPM pulse. Making use of SiPM-ASIC systems we study the costs and effects of applying an event energy discrimination scheme to control the volume of produced data by the detector modules. For this analysis, our researching approach consisted on the implementation of filter versions with different levels of accuracy in the event differentiation. Our filter designs present an increasing degree of complexity as the filtering accuracy grows. For each of these implementations, we analyze the effect on the system count rate while monitoring the preservation of the resulting energy and time resolutions.

The initial hypothesis that motivates this work sustains that on-line energy discrimination is an effective and lightweight solution to cope with the BW limitation issue present in most highly pixelated PET scanners. This research poses iterative objectives to confirm our hypothesis:

1. Study on a reference system the energy distribution of the received events to identify on the events energy space the areas to filter or to preserve.
2. Define internal hardwired filter limits according to the observed energy distribution.
3. Implement different versions of the filter with increasing levels of accuracy and resources costs.
4. Analyze the evolution of system count rate as a function of filter thresholds for the different filter versions along with their implementation costs.
5. Check possible changes on system performance: energy and time resolutions.

2. Methods

This section goes through the description of the implementation chosen to overcome the BW limitation problem along with the equipment and experiments used to analyze the solution.

2.1. General considerations on filter implementation

Applying no on-line energy filter, the DAQ system transmits to the PC every single gamma event that the ASICs produce. The acquisition software processes this data discarding any event whose time or energy stamp lay out of the defined limits. Given the accessibility from the readout electronics to the events time and energy information, we decided to implement the on-line energy filter on the front-end electronics reading the ASICs. Filtering at the first level of the DAQ would already reduce the volume of data transmitted from the detector modules to the PC. Thus, easing any possible BW limitation between the on-detector DAQ electronics section and the off-detector DAQ electronics section on the data collector. Even though the number of received events decreases, if the filter thresholds defining the acceptance window are properly set, the system would preserve its sensitivity.

The TOFPET ASIC[10] uses the time-over-threshold (TOT) technique to compute the energy of the gamma events. For every detected SiPM pulse the ASIC encapsulates the information of the gamma event in a digital packet. This information includes two time stamps used to calculate the TOT. Each of this two stamps contains in turn two sub time tags: coarse and fine. The coarse one has a 6.25ns time binning and the fine one 50ps. Through the use of the fine time information we achieve the accuracy required for Time-of-Flight (TOF) PET applications in the measurement of the time of arrival of gamma photons. In the same way, when we use the fine time information to compute the TOT, we get a higher accuracy in the measure of the events energy than using just the coarse time information. But there is no need to achieve such a degree of precision for a first level on-line energy discrimination. For that reason, the filter implementations analyzed in this study ignore the fine time information and perform an energy discrimination based on the coarse time information. In practice, the on-line energy filter subtracts the coarse time stamp associated with the instant when the rising edge of the SiPM pulse surpassed the threshold set by the ASIC (T_{coarse}) to the one associated with the instant when its falling edge falls behind the threshold (E_{coarse}). As a result, the following equation 1 defines the general expression to compute the event coarse TOT value. This is the value to compare against the defined energy window limits during the on-line event discrimination.

$$\begin{aligned} event_coarse_TOT &= \\ &= event_E_coarse - event_T_coarse \end{aligned} \quad (1)$$

Pixelated systems integrate hundreds or thousands of detecting channels, where each of them present different properties in function of its SiPM pixel and ASIC channel. Because not every SiPM pixel, nor every ASIC channel, presents the exact same performance. Both these two factors contribute to the non-uniformity of the system response. The solution to this problem lays in the calibration process. For every system channel and for the whole energy range, the energy calibration process[9] obtains a list of equivalences between coarse TOT values and their corresponding energy. The software post-processing uses this information to treat the data read from the detector. For the firmware implementation of the filter contained in the front-end electronics FPGAs, we decided to start by designing an uncalibrated version of the filter followed by its calibrated counterpart. The uncalibrated one ignores the energy calibration information setting the same energy thresholds, which define the acceptance window, for all the channels. Whereas the calibrated one reads the energy calibration file setting a particular pair of thresholds for every single channel. This incremental implementation approach gave us the possibility to begin with a quick proof of concept of the filter using the simpler and faster-to-implement uncalibrated version. With this first version, we could refine the on-line energy filter design. Once we finished the first stage of testing and tuning, we focused our efforts during the implementation of the calibrated filter on calibration related issues.

2.2. Equipment

The on-line energy filter aims to ease the large data volume produced on a highly pixelated PET system. Specifically, our original goal was to cope with the bandwidth limitation issue present on the EndoTOFPET-US system, a PET scanner with 4096 channels producing an aggregated data rate of 40MHz. Experiments with this equipment show how this 40MHz of valid gamma events comes along with a big proportion of low energy events (noise events) increasing the resulting system output rate. The DAQ can drop these events with no detriment on the resulting system sensitivity because their energy is too low and thus they are not useful for the image reconstruction.

Given the status of the EndoTOFPET-US system, which was lacking its commissioning and calibration, we decided to test the filter performance on a similar but already working system, the PETsys demonstrator[11]. This PET system uses the same readout electronics than the EndoTOFPET-US but with a different topology. The demonstrator integrates 2048 detector channels geometrically disposed on a small ring of detectors. Despite the differences between the two systems, all the influential characteristics for the energy filtering are the same and thus the conclusions obtained through the analysis of these tests on the demonstrator will be valid for the EndoTOFPET-US as well.

2.3. Uncalibrated energy filter

The uncalibrated energy filter implementation sets common filtering limits for all the system channels. Depending on the system response, the user defines appropriate coarse TOT values to specify these limits. Current section covers not only the implementation details of this common limits version of the filter but it goes through the optimization process of the filter as well.

2.3.1. Implementation details

The complete filter implementation consists of two firmware modules plus a SW script. The python SW script makes use of PETsys electronics libraries to configure and initialize ASICs and DAQ front-end modules with default parameters or the ones obtained from calibration[9]. Then the script sends a filter configuration command to every active DAQ front-end module setting the upper and lower thresholds that define the acceptance energy window of the module's filter. Upon complete system and filter configuration the script reads data through the acquisition system.

SiPM TOT-energy relationship is strongly non-linear[12] and every system channel present different performances. For every energy value of each channel the equivalence energy-TOT changes. Thus, it would make no sense to express the filter thresholds in terms of energy for the uncalibrated version. For this first implementation the filter, thresholds set by SW are directly expressed in time as coarse TOT values. And the filter accepts those events whose coarse TOT lays between the temporal thresholds set on the filter, independently of the actual energy that it represents. As a consequence, there would be one single pair of thresholds to set for all the system channels.

The DAQ system design included the definition of a set of configuration and control commands. The acquisition SW sends these commands to the DAQ front-end modules during the configuration phase[9]. For the filter implementation, we extended the configuration command space to include a new command for the filter thresholds setting. This command accepts two 10 bits numerical parameters, one for the lower threshold and one for the upper one. Even though the user specifies the filtering limits in seconds, ASICs coarse time tags come in CLK cycles. Hence, the SW script converts the parameters defining the filtering limits to clock cycles to avoid unnecessary operations on firmware, we compare these values against the incoming event coarse TOT. Given the 160MHz used to clock the system, the SW divides and rounds the thresholds given in seconds by 6.25ns to set the thresholds directly expressed in CLK cycles. Given the 10bits length of the ASIC coarse time stamps, the 10bits thresholds parameters cover the full span of coarse TOT.

Filter firmware modules are responsible for handling its configuration commands and for the on-line filtering of incoming gamma events based on their energy. When a filter threshold-setting command arrives to a DAQ front-end module, the FPGA configuration logic block extracts the thresholds from the configuration command and passes them to the on-line energy filter stage. During the detector configuration phase the FPGA stores the thresholds on a register and it reads their values upon each gamma event arrival during the filtering stage. The on-line filtering process consists on the continuous inspection of incoming ASIC data packets. For every gamma event contained in the data packet, the filter computes the event coarse TOT, compares it against the given energy thresholds and takes the filtering decision. If the event coarse TOT lays outside the acceptance energy window the filter removes the current event from the data packet, sending to the DAQ collector module packets containing all the valid gamma of events of the original data packet.

ASICs send data packets with all the detected gamma events every $6.4\mu s$, i.e. every 1024 CLK cycles. Internally, the DAQ system formats the incoming ASIC data packets to deal with 64 bits words. Each 64 bit word contains either a packet header word or a single and complete gamma event and the firmware handles each word as a whole, it implements a 64 bit architecture. The firmware

data reception module writes 64 bits words of the data packet on a buffering FIFO placed right before the on-line filtering stage. This is a 64 bit wide FIFO with a capacity for 1024 words. The ASIC handles 8 bits words, implementing a 8 bit architecture, thus the DAQ front-end module processes data packet 8 times faster given its 64 bit architecture. As a consequence, the DAQ front-end module compacts the back-to-back data packets produced by the ASIC and sent as a continuous data stream. Thus in the front-end FPGA the firmware processes the incoming data stream on a non continuous burst mode. The event discriminator module reads a word from its input FIFO every time a new word is available and it has finished processing the previous one. DAQ front-end modules need a CLK cycle to process each data packet word but complete processing of a data packet by the uncalibrated energy filter takes one more CLK cycle. Given the non continuous packet handling, where at most data packet processing takes 128 CLK cycles, the on-line energy filter module has at its disposal 896 free CLK cycles. Thus, the extra CLK cycle for a data packet processing will not incur on a problematic delay.

The DAQ front-end modules house the two firmware components for the on-line energy filter. While the DAQ collector module needs no adaptation as the filter functionality is transparent to it. Filter configuration commands use the common format of front-end configuration and control commands. Thus, DAQ collector module, who takes care the front-end control and configuration of as well, merely retransmits these commands towards the addressed front-end unit. And from the point of view of data collection, the filter makes nothing but removing events which are not in compliance with the energy rules without modifying the data packet format. As a result, the DAQ collector module needs no modifications, it processes filtered data packets as if it were any regular data packet.

2.3.2. Optimization

Upon the first acquisition making use of the demonstrator system and thorough the study of the energy space of the acquired gamma events, we noticed that the TOFPET ASIC produces some events with wrong time stamps which lead to a coarse TOT out of the expected range. The coarse TOT map in Figure 1 shows the energy distribution of all the gamma events obtained on a 5min acquisition with a Na22 point source centered in-

side the detector ring without any filtering. This graph exhibits the malfunctioning of 5 ASICs on the system. These are ASICs with channel IDs: 64-127, 192-255, 320-383, 1088-1151, 1472-1535; where channel IDs between 0 and 1023 belong to the first DAQ front-end module and between 1024 and 2047 to the second one. These five noisy ASICs produce a big number of events scattered over the whole energy space. Analyzing a detailed view of the region of interest (coarse TOT between 0 and 70 CLK cycles) depicted in the lower plot of the coarse TOT map in Figure 1, we noticed that, despite being faulty ASICs, they still produce a bigger number of events in this region where their energies follow the same distribution as the one present in the non faulty ASICs channels. This means that, although identified as malfunctioning ASICs, these ASICs produce valid data to preserve mixed with wrong time stamps events. The upper picture on the coarse TOT map of Figure 1 shows how the rest of the ASICs produce some events out of range too. This data visualization indicates how an on-line energy filter would optimize the system BW usage. The filter would reduce the system's output data rate by filtering the high concentration of low energy events considered as non-useful events. Further, this discriminating stage will decrease the rate even more dropping all the events cataloged as events with a wrong energy information. Data shown on the TOT map of Figure 1 illustrate how the demonstrator used for this study contains malfunctioning ASICs producing such incorrect events.

The full range coarse TOT map on the upper picture of Figure 1 conveys other important information too. The accumulation of events in the negative coarse TOT region close to zero indicates that for some events E_{coarse} is slightly smaller than T_{coarse} . According to the working principle of the ASIC this scenario should not arise. However, small length differences on the TOFPET ASIC electrical routes could cause deviations from the actual TOT. This discrepancy with the real difference between E_{coarse} and T_{coarse} could generate events with a negative coarse TOT close to zero for the events with the smallest energies. Furthermore, there is another abnormal concentration of events. Some events build-up in the negative coarse TOT zone close to -1024 CLK cycles, i.e. E_{coarse} close to zero and T_{coarse} close to its maximum value. The reason for it to happen is what we call the counter rollover effect. Internally the TOFPET ASIC uses a 10bits free-running counter for the time tagging of

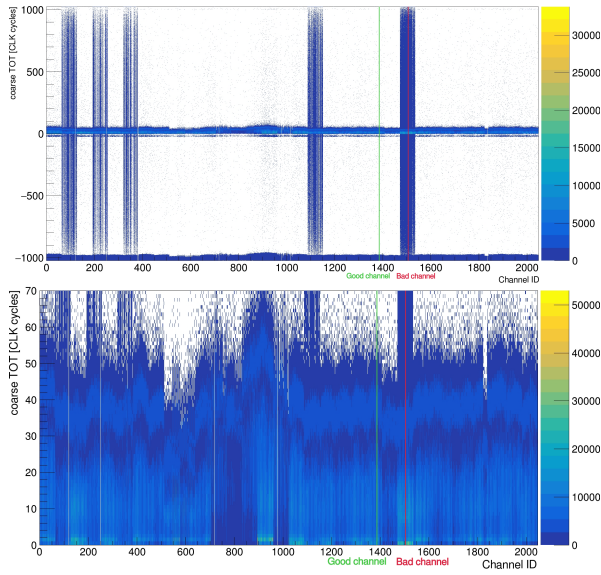


Figure 1: Coarse TOT distribution of the received ASICs events for the 2048 system channels expressed in CLK cycles, 6.25ns. The produced events are the result of a 5min acquisition placing a Na22 point source centered on the detector ring. The upper plot shows the complete coarse TOT span and the lower one focuses on the region of interest corresponding to the valid energy range. Both plots identify two reference channels used on our study: the “Good channel” and the “Bad channel”. These channels correspond to the system channels with the smallest and the biggest amount of noise respectively.

E_coarse and T_coarse. If T_coarse gets a value of the counter when is about to roll back to its initial value (i.e. T_coarse close to 1024), then E_coarse would get a value of the counter shortly after rolling back (i.e. E_coarse close to 0).

We pursued an optimization of the on-line energy filter based on the information obtained from the study of the events energy space. We selected two reference channels to compare the results of the different refinements: the “Bad channel” and the “Good channel”. We selected the “Bad channel” as the system channel producing the biggest number of events, thus the noisiest system channel, which corresponds with one of the channels of a malfunctioning ASIC. Channel 1506 is the reference “Bad channel”. In opposition, the reference “Good channel” is the one producing the smallest amount of events, which corresponds with the less noisy channel (i.e. the one with less events with an energy outside the valid energy range). We chose channel 1390 for this purpose.

The method chosen as a first assessment of the optimization process is a visual comparison of the energy distribution of the data acquired by the two reference channels. For this purpose, we plot the T_coarse VS E_coarse distribution of the events received by a reference channel. The T_coarse VS E_coarse plots on Figure 2 show the resulting reference maps for the “Bad channel” in the right-side graph and for the “Good channel” in the left one. Through the filter optimization process we intend to get rid of the events cataloged as noise. As a consequence, the newly obtained T_coarse VS E_coarse plots of the “Bad channel” should be alike the reference “Good channel” map after optimization.

SW like. Correct identification and preservation of events with valid but misleading energy information is the key to preserve system sensitivity. Thus, the optimization goal is to exclude the events with a non-valid energy value while keeping the events which, despite containing meaningful energy information, lead to a coarse TOT computation laying outside the valid range due to TOFPET ASIC particularities.

The acquisition SW already deals with wrong energy stamps taking into account the ASIC characteristics. This SW performs a preprocessing of the received data discarding all the events which present negative energy values close to zero due to ASIC inter-path length differences. We discard these events as they are noise events with an en-

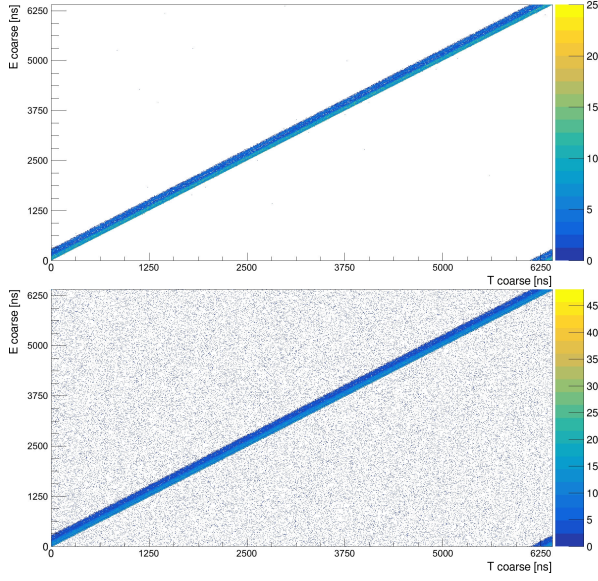


Figure 2: E_coarse versus T_coarse distribution of the received ASICs events expressed in ns. The produced events are the result of a 5min acquisition placing a Na22 point source centered on the detector ring. The upper plot shows distribution for the reference “Good channel” and the lower one the distribution for the “Bad channel”

ergy close or equal to zero. Events preprocessing also takes care of the events whom suffered the counter rollover effect on their time tagging. For these events, the acquisition SW recomputes their resulting TOT by adding 1024 CLK cycles to the default TOT computation. Given the 10 bits size of the coarse time counter, this operation corrects the error introduced by the rollover effect obtaining the appropriate TOT of these events.

The first optimized version of the filter replicates the SW preprocessing, thus we identify this filter version as “SW like”. Instead of using the default coarse TOT computation defined by equation 1, the “SW like” implementation introduces the same conditions used by the SW preprocessing for its computation. Replicating SW preprocessing conditions we differentiate counter rollover effect events by a coarse TOT smaller than -256 CLK cycles. The DAQ front-end filtering module computes the coarse TOT of these events according to equation 2.

$$\begin{aligned} coarse_TOT &= 1024 + E_coarse - T_coarse \\ \iff (E_coarse - T_coarse) &< -256 \end{aligned} \quad (2)$$

If this condition is not met, then the filter checks if the event needs coarse TOT correction for inter-

path length differences. The DAQ front-end modules recognize this scenario when E_coarse is smaller than T_coarse while counter rollover conditions are not met. For this case, the filtering module uses a modified coarse TOT computation to approximate their energies to zero as expressed in the coarse TOT equation 3. A zero coarse TOT assignation causes the events filtering for any low threshold setting different from zero.

$$\begin{aligned} coarse_TOT &= 0 \iff \\ -256 &\leq (E_coarse - T_coarse) < 0 \end{aligned} \quad (3)$$

The T_coarse VS E_coarse plot on Figure 3 shows the effect that the optimization produces on the “Bad channel”. Comparing this result with the one depicted in the T_coarse VS E_coarse plot on Figure 2 for the non-optimized case, we observed how the first optimization clears some noise while preserving the events who suffered the counter rollover, events in the bottom right corner of the plot. Nevertheless, this T_coarse VS E_coarse plot shows how the filter could clear much more noise by the refinement of the frontier value differentiating the counter rollover events, i.e. the -256 CLK cycles frontier.

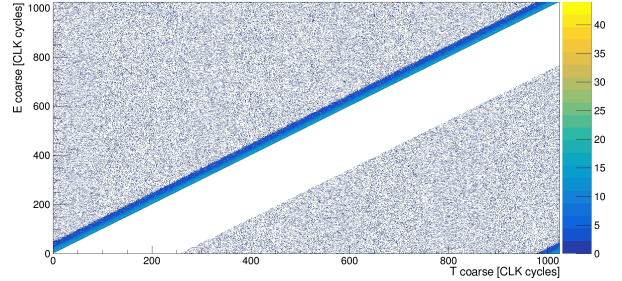


Figure 3: E_coarse versus T_coarse distribution of the received ASIC events produced on the reference “Bad channel” expressed in CLK cycles, 6.25ns. The received events are the result of a 5min acquisition placing a Na22 point source centered on the detector ring when DAQ front-end module implements the “SW like” version of the filter.

The filter does not alter the event information, it merely reads the event coarse time stamps to compute its coarse TOT value for internal comparison against the energy window limits. The events, whose energy meets the acceptance conditions, pass the on-line filter unmodified. Once the filter module identifies an event with a distorted energy due to one of the two ASIC special cases, it would be simple to modify the event coarse time stamps on the fly to compensate the effects of these cases.

Nonetheless, we decided to leave the stamps untouched on the first filter implementation to avoid introducing any firmware artifact in the system performance.

New rollover limit. According to the results of the “SW like” implementation, SW preprocessing fails to properly adjust the counter rollover case limit conditions. Next filter optimization step consists in the correct adjustment of this limit. Thus, we refer to this new implementation as the “New rollover limit” version.

To select the optimum coarse TOT limit value that keeps the counter rollover events while filtering out the rest of the events with a negative coarse TOT, we studied the coarse TOT distribution for the case of the channel producing in average the highest TOT values. This way, we avoid setting an upper limit that would cut some valid events for the channels producing events with coarse TOTs which in average are higher than the ones produced by the reference channel. We designate this new reference channel as highest TOT channel. The coarse TOT distribution of Figure 1 illustrates how the ASIC with channel IDs [896:956] generates events with higher coarse TOT values. Out of these channels, 925 is the one producing the highest coarse TOTs. Thus channel 925 is the one selected as the reference “Highest TOT channel”.

We performed five acquisitions and analyzed the their coarse TOT distributions obtained for the “Highest TOT channel”. Due to the consistency of the results five acquisitions where enough to select the limits. The full span coarse TOT distribution in the upper plot of Figure 4 illustrates how, for the reference channel, most of the events lay in the region $coarse_TOT = [0, 80]$ CLK cycles. Events in this region do not undergo any of the TOFPET ASIC particularities. This histogram also shows a smaller concentration of events in the area $coarse_TOT = [-1024, -950]$. The events with energy values within this region are the ones which suffered the counter rollover effect on their time stamping. For every acquisition, observing the distribution of events in this region of the plot, like shown in the lower coarse TOT detail of Figure 4, we extracted the maximum coarse TOT value found on this region to define the counter rollover limit. We obtained the limit value used by the filter by adding a three CLK cycles margin to this maximum coarse TOT value found out of the five acquisitions. As a result, we set the counter rollover coarse TOT

limit to -950 CLK cycles. Adding a wider margin of CLK cycles would imply filtering less noise events but adding a smaller one could cause the filtering of meaningful counter rollover events. We chose 3 CLK cycles to balance these scenarios.

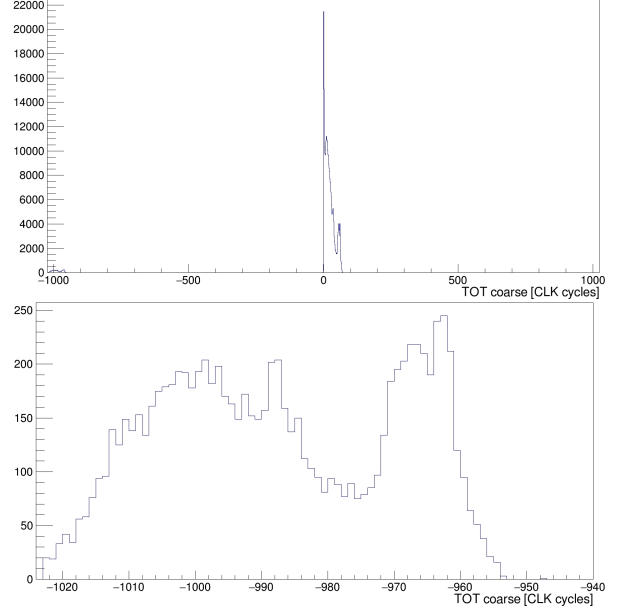


Figure 4: Coarse TOT histogram produced by the received ASIC events for the reference system channel producing the highest coarse TOT values, channel number 925. We express coarse TOT in CLK cycles, 6.25ns steps. The produced events are the result of a 5min acquisition placing a Na22 point source centered on the detector ring. The upper hand plot shows the complete coarse TOT span and the lower one focuses on the TOT region of the events suffering the counter rollover effect.

Using this information, we altered the coarse TOT computation for the TOFPET ASIC special cases. Obtaining for the “New rollover limit” filter version the following new coarse TOT rollover case equation, equation 4, and the new coarse TOT path length differences case equation, equation 5:

$$coarse_TOT = 1024 + E_coarse - T_coarse \quad (4)$$

$$\iff (E_coarse - T_coarse) \leq -950$$

$$coarse_TOT = 0 \iff$$

$$-950 < (E_coarse - T_coarse) < 0 \quad (5)$$

Making use of the new filter implementation we run a new acquisition from which we obtained the T_coarse VS E_coarse distribution of Figure 5. This

new distribution shows the effect that the rollover limit optimization produces on the “Bad channel”. Comparing this result with the T_coarse VS E_coarse plot depicted in Figure 3 for the “SW like” version, we observed how the optimization clears most of the noise in the $E_coarse < T_coarse$ region while preserving the events who suffered the counter rollover effect. Still we could free much more noise refining the filter optimization for the $E_coarse > T_coarse$ region.

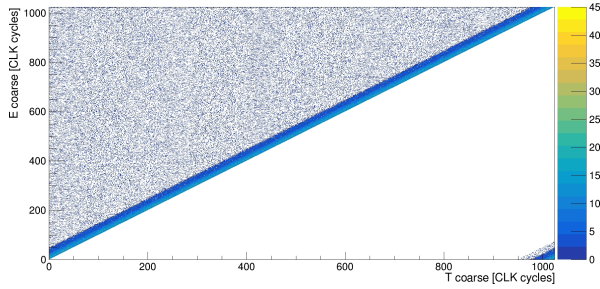


Figure 5: E_coarse versus T_coarse distribution of the received ASIC events produced on the reference “Bad channel” expressed in CLK cycles, 6.25ns. The received events are the result of a 5min acquisition placing a Na22 point source centered on the detector ring when the DAQ applies the “New rollover limit” implementation of the filter.

New limit + up bound. In the light of the results obtained with the “New rollover limit” implementation, we decided to set another hardwired coarse TOT limit. This time, we will look for an upper limit on the events acceptance which would eliminate the noise events laying in the $E_coarse > T_coarse$ region.

The methodology followed to select an appropriate fixed upper limit for the filter imitates the one used for the counter rollover boundary choice on the “New rollover limit” version. We performed five acquisitions and analyzed the energy distribution on the reference “Highest TOT channel” within the region of interest, i.e. $coarse_TOT = [0, 80]$. The coarse TOT plot of Figure 6 shows an example of the kind of histograms used for the analysis. Once again, the coherence of the results between acquisitions lead us to limit the number of runs to five. For each acquisition we recorded the biggest coarse TOT value as the upper bound of the current acquisition. To select the definitive upper bound for the filter we added a three CLK margin to the maximum of the recorded values. We selected this margin according to the same criteria as for the previ-

ous optimized version: balance of noise reduction versus data loss.

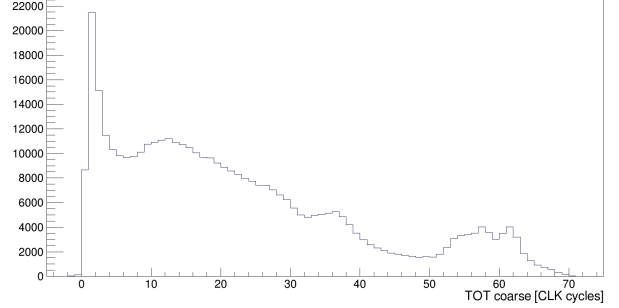


Figure 6: Coarse TOT histogram produced by the received ASIC events for the “Highest TOT channel” system’s reference channel expressed in CLK cycles, 6.25ns. The produced events are the result of a 5min acquisition placing a Na22 point source centered on the detector ring. The plot focuses on the valid energy range.

The new filter optimized version sets to zero the coarse TOT of the events surpassing the upper limit as shown in the new coarse TOT equation for high energies, equation 6. On the filtering stage the DAQ deletes from the data packet all events with a zero coarse TOT, including those who exceeded the upper limit, when using any low threshold setting different from zero.

$$\begin{aligned} coarse_TOT = 0 &\iff \\ (E_coarse - T_coarse) &\geq 80 \end{aligned} \quad (6)$$

Once applying the last optimization to the filter, the coarse TOT distribution of the events in Figure 7 shows how we eliminate all the noise that can be cleared out using the same unique fix margin for every channel and making sure that the filter does not cut any relevant event, even for the channels producing the highest TOT values.

2.4. Calibrated energy filter

Given the differences in the performances of the detector channels, the system requires a calibration process to homogenize the response of the 2048 channels. This calibration process includes the energy calibration which relates TOT and its equivalent energy for every system channel and for the complete energy range ($coarse_TOT = [0, 6.4\mu s] = [0, 1024 CLKcycles]$). The calibrated filter version exploits the energy calibration information to set independent filter thresholds adjusted for every particular channel according to their response. As a

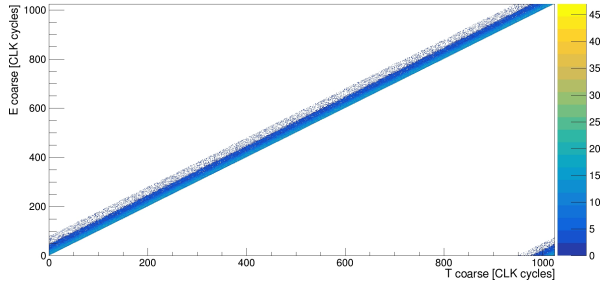


Figure 7: E_{coarse} versus T_{coarse} distribution of the received ASIC events produced on the reference “Bad channel” expressed in CLK cycles, 6.25ns. The received events are the result of a 5min acquisition placing a Na22 point source centered on the detector ring when the DAQ applies the “New limit + up bound” filter implementation.

consequence, we define the calibrated filter thresholds as real energy values expressed in electron-volts [eV]. We will need to translate these values using the energy calibration table to extract the equivalent TOT thresholds of each channel.

2.4.1. Implementation details

This TOT-energy relationship is strongly non-linear and we cannot model it analytically. Thus, the calibration process obtains this relation experimentally by measuring the resulting TOT from gamma photon sources with photo-peaks of known energy. Experimental data shows an exponential TOT-energy relation, being able to fit most of the system channels with an exponential function. Nonetheless, the calibration results used by the SW processing and configuration modules are not just a set of parameters to define the exponential function fitting each channel but instead we use a complete table. This table relates TOT and energy for each channel and for a subrange within the expected energy range. This ranges goes from $TOT = 0$ up to $TOT = 499.5ns$ on 0.5ns steps. According to experimental results $TOT = 499.5ns$ corresponds to a value around 100MeV for most of the channels. Hence, there is no need to cover the full TOT range (up to $6.4\mu s$) given our energy range of interest, i.e. around 511keV. Even though the calibration procedure could compose a smaller TOT-energy table with values up to an energy value closer to the energy of interest (around 1MeV for example), PET-sys decided to expand the table to higher energies to introduce a margin for the ASICs channels producing the highest TOTs.

We modified the filter SW script for the calibrated version to configure independent energy

thresholds for every system channel upon loading the main ASICs and front-end boards configuration parameters. For the filter configuration, we pass two parameters to the script specifying the lower and upper thresholds expressed as an energy value in keV. These thresholds define the filter energy cuts or acceptance window. For each system channel the script reads the TOT-energy table searching for the closest energy value to the lower threshold value passed to the script. Then, it obtains the TOT value associated to such energy value for that particular channel. Once the script identifies the lower threshold, it keeps reading the table entries of the channel under analysis until it finds the closest energy value to the higher threshold value passed to the script obtaining its equivalent TOT value. The script then constructs a configuration command containing the two TOT filter cuts for the channel under process. In the configuration command we express the threshold value to send as number of CLK cycles, like for the uncalibrated filter version, because the ASIC data packet uses the same units and thus we avoid extra firmware processing. The SW script repeats this procedure for each channel to configure the on-line energy filter thresholds of every system channel independently. Once the configuration SW sets all the system parameters including the filter ones, the acquisition SW reads data through the DAQ system. In some cases, the calibration points obtained for a certain channel do not permit a correct function fit with an exponential function. The configuration SW identifies those channels which failed the calibration process when it notices a non-positive tendency while reading the TOT-energy table. For these channels the script configures the threshold values used for the previous channel configured who has a valid TOT-energy function fit. When the user requests too low or too high threshold values, for some channels their TOT-energy entries do not reach the given threshold values and thus the limits used for these channels are the ones used for the previous channel configured who has an equivalent TOT for the given energy threshold. Channels using filter limits of a previous channel are characterized by TOT values above or below the average TOT values for the current setup.

The new filter implementation uses different threshold values for each channel and thus its configuration command syntax changes to include the channel address. As a result, the calibrated filter configuration command follows this syntax:

- A header byte to identify the command type, which indicates that this is a filter threshold setting command.
- A 10 bits word containing the channel ID.
- A 10 bits word containing the lower threshold value in CLK cycles.
- A 10 bits word containing the upper threshold value in CLK cycles.

Though the system contains 2048 channels, the channel ID parameter of the configuration command contains 10 bits instead of 11 because it needs to identify the channel within the front-end module which contains 1024 channels. The communication protocol between DAQ collector module and front-end modules encapsulates the filter configuration command using a header that already identifies the destination front-end module.

For the threshold values storage, on each front-end module the firmware implements a 20bits wide Look Up Table (LUT) with 1024 entries, one for each of its channels. This LUT is 20bits wide to store both the lower and upper thresholds for each channel entry. The filter firmware module responsible of configuration commands processing unpacks the configuration command extracting its destination channel ID and thresholds. It uses the channel ID as the LUT address and writes its threshold values. During the configuration phase this module receives the 1024 configuration commands from the configuration SW script to fill the complete table of that particular front-end module.

During the acquisition phase, the on-line energy filtering discriminating stage continuously inspects the incoming ASICs data packets. The filtering module extracts from the packet information from individual gamma events and for each of them the processing consists in the following steps:

1. Read the event channel ID and time stamps.
2. Compute the event coarse TOT according to the rules defined during the filter optimization process.
3. Read the LUT using the event channel ID for addressing.
4. Compare the event coarse TOT against the threshold values read from the LUT.
5. If the event coarse TOT lays within the acceptance window, the filtering stage let the gamma event pass through including them in the filtered

data packet. But when the coarse TOT does not meet the acceptance conditions the filter removes the event from the data packet sent to the DAQ collector module.

Reading from the LUT the channel energy thresholds defined for the filtering takes two more CLK cycles for the processing of each gamma event. And as for the uncalibrated filter version, the complete processing of the data packet takes one more CLK cycle. Given the different architectures implemented by the ASICs and the DAQ front-end module, as explained in the uncalibrated filter implementation Section 2.3.1, the filter has at its disposal 896 CLK cycles for the extra processing time that it needs. Hence, the filter could deal at most with 447 events per data packet, 70Mevents/s, causing no problematic delay. Simulations show how this kind of electronics will produce no more than 10Mevents/s per DAQ front-end module, which leads us to the conclusion that the on-line energy filter can absorb the volume of data produced by the detector modules on the fly. For the system under study and our experiment conditions, i.e. a $24\mu\text{Ci}$ source centered on the demonstrator detector ring, the system produces a peak event rate of 190 events per second. Having two DAQ front-end detector modules present on the system, each one sustains a 95 events per second peak rate which is well below the on-line energy processing capacity.

The calibrated version of the filter has no special requirements on the DAQ collector module. The front-end modules FPGAs contain both the configuration and on-line processing firmware modules. The DAQ collector forwards the filter configuration commands and processes the incoming filtered data packets as it does for any other configuration command or data packet.

2.5. Experiments and laboratory methods

For the characterization of the on-line energy filter performance our experiments emulated a real PET acquisition scenario. A Sodium-22 (Na22) point source placed in the center of the demonstrator detector ring was radiating uniformly over the detectors surface on our experiments. Na22 sources are positron emitters in the same way as the radioactive isotopes used for PET tracers are. Once a positron annihilates with an electron, the process emits two back-to-back gamma photons with a 511keV energy. The acquisitions in our experiments target the detection of these gamma rays as

in real PET acquisitions. Having a source illuminating the detectors with the right energy, we can observe through the acquisitions with the on-line energy filter if the DAQ preserves data in the valid energy range while filtering out all the noise produced outside this range.

Our main goal is to reduce the excess on the data volume produced by the system and thus our experiments analyze the influence of the filter on the system's output data rate. For the different filter implementations, our experiments analyzed the progressive data reduction obtained with each successive version. First filter versions pursued an optimization of its internal hardwired limits which ensure to clear out all gamma events with an energy value out of the valid range. Hence, for the study of the data reduction achieved through the optimization process, we set no filter thresholds measuring the contribution obtained by each optimization step. Secondly, we studied the data reduction obtained through the tuning of the filter's low energy threshold. In this second set of experiments, for the different filter versions, we performed a low energy threshold sweep analyzing the resulting data output rate. We perform all the experiments under the same conditions to have a common framework for the results comparison. Experiments maintain a constant acquisition time and use the same radioactive source. Preserving these two experiments conditions we ensure that the volume of data produced by the detector modules remains constant.

An efficient data reduction process preserves the resulting system sensitivity which directly affects on the system's performance. The filter should not reject any event useful for the image reconstruction, throwing away only those events whose energy is either too low or too high to belong to a gamma photon event. To prove the conservation of the system's performance, in our final experiment we placed the Na22 source centered in the detector ring and performed a long enough acquisition to get good statistics for the data analysis of the system's energy spectrum and CTR distribution. Specifically, using a Na22 source, whose estimated activity is $24\mu Ci$, we found that 10min acquisitions were needed to achieve enough statistics to produce smooth and contiguous histograms.

2.6. Statistical methods

The conclusions obtained from our tests are not based in the result of one single acquisition per

experiment. To reduce the uncertainty in the results outcome, we performed several acquisitions for every experiment. From these acquisitions we extracted their average values and variabilities and used them to express our results. Given the consistency of the results we decided to limit the number of acquisitions per test to 5.

For the statistical data analysis and its visualization we used ROOT, a data analysis framework developed at CERN for statistical analysis and visualization. Through this framework we read the gamma events database created with each acquisition, extract the event's feature or features of interest for the experiment and visualize the data in the form of 1D or 2D histograms showing the distribution of the values received for the parameters under study.

3. Results

This section describes the results obtained making use of the two different versions of the on-line energy filter described in the methods Section 2. We used the acquired data to analyze the non-valid data rate reduction given through the filter optimization process and by the filter thresholds tuning. During the results analysis we studied the resources consumption cost for the inclusion of the different filter versions on the system.

3.1. Uncalibrated energy filter

As a result of the optimization process described in the uncalibrated filter methods Subsection 2.3.2, three different implementations of the on-line energy filter were obtained before reaching the best solution. Setting no thresholds on these filters and measuring the obtained data rate would give us the contribution of each optimization step to the non-valid data rate reduction. For each implementation of the optimized uncalibrated filter we performed five acquisitions during one minute each, setting the Na22 source centered in the detectors ring. Under the same experimental conditions but using no filter we ran five acquisitions to get the reference volume of data for comparison. The comparative column chart on Figure 8 illustrates the data reduction obtained through the different optimizations of the filter. For each implementation we computed the average value of the 5 acquisitions and compared against the reference non filtering case to get the percentage of the data volume reduction. Error

bars illustrate the variability of the data volume for acquisitions under these circumstances.

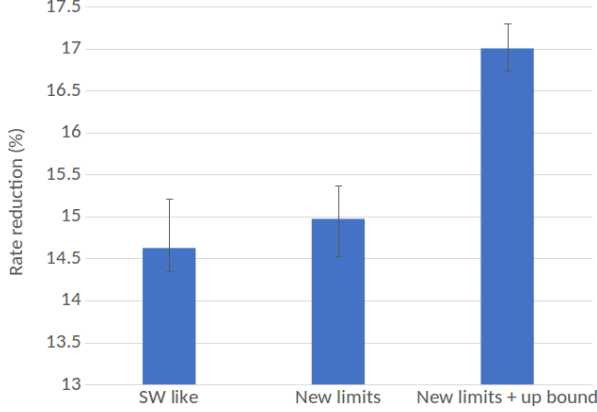


Figure 8: Rate reduction obtained with the uncalibrated filter through its optimization process. We express the rate reduction as a percentage relative to the reference non filtering case.

Setting no filter thresholds, this experiment gives us the raw contribution of the optimization setting the filter hardwired limits. The comparative column chart on Figure 8 shows us how the first optimization step produces a relevant reduction in the incoming data rate of 14.5%. This graph exhibits too the small contribution to this reduction given by the successive refinements tuning the filter hardwired limits to its optimum values. The second optimization implementation, “New rollover limit”, adds a 0.5% to the previous rate reduction, reaching a 15% rate reduction. The last optimization step, “New limit + up bound”, presents a rather small contribution but still bigger than the one given by the “New rollover limit” version obtaining now 17% less data than in the non filter case. To understand the meaning of these results we need to bare in mind the coarse TOT distribution shown in Figure 1. Apart from the events identified as valid events undergoing counter rollover effect present in the region $-1024 < coarse_TOT < -950$, the biggest concentration of events outside the valid energy range is in the area $0 < coarse_TOT < -50$ which concentrates the low energy events who suffered the effect of the ASIC inter-path length differences. These non-valid events are already filtered on the first optimization step by the “SW like” version. Thus the “SW like” implementation is the version with the biggest contribution to the rate reduction. In the other two implementations rate reduction is mainly given by the filtering of the non-valid events belong-

ing to one of the five problematic ASICs identified on the system. The bigger the number of problematic ASICs present in the system, the higher the rate reduction for the last two filter optimizations.

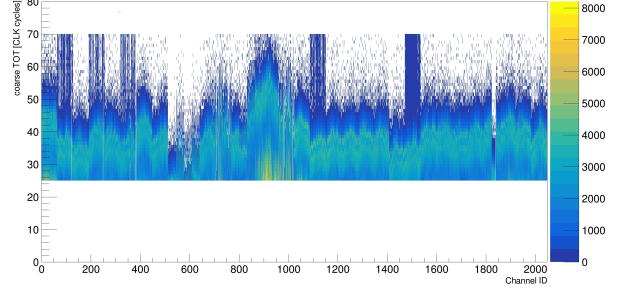


Figure 9: Coarse TOT distribution of the received ASICs events for the 2048 system channels expressed in CLK cycles, 6.25ns. The produced events are the result of a 5min acquisition placing a Na22 point source centered on the detector ring when using the optimized version of the uncalibrated filter on the DAQ and setting 25 and 70 CLK cycles as the filtering thresholds.

Once we optimized the filter setting the optimum hardwired filter limits, we performed a threshold sweep searching for the best TOT thresholds to apply on all the channels simultaneously. The coarse TOT distribution on Figure 9 depicts the result of applying the threshold values found to conserve the valid events of every channel, even for those with a lower or higher coarse TOT than the average. Hence, the resulting lower threshold for the uncalibrated filter was 25 CLK cycles and 70 CLK cycles for the upper one. During the threshold sweep we recorded system’s output data rate obtaining the rate evolution curve depicted in Figure 10. Through this experiment we observed how setting the optimum thresholds on the uncalibrated filter, the ones used to get the coarse TOT distribution of Figure 9, we achieve a 70% data rate reduction while conserving all the events with a valid energy.

We studied the resources consumption on the DAQ front-end module FPGA implementing the filter to judge the implementation complexity of this uncalibrated filter version. The uncalibrated filter consumes for the implementation of the filtering module plus the changes on the configuration module the following FPGA resources for our device under use, Xilinx Kintex7 XC7K160T:

- 278 slice LUTs, 0.27% of the total number of slice LUTs in the device.
- 510 slice registers, 0.25% of the total number of slice registers in the device.

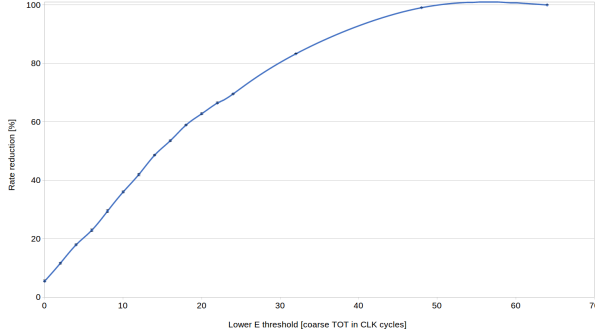


Figure 10: Rate reduction obtained through the increment of the low filter threshold when applying the optimized version of the uncalibrated filter on the DAQ. We express the rate reduction as the percentage relative to the reference non filtering case.

- 119 slices, 0.47% of the total number of slices in the device.

3.2. Calibrated energy filter

The calibrated implementation of the filter adjusts the thresholds independently for each channel based on the information provided by the energy calibration. The filter energy cut will be different for every channel, according to their individual equivalent coarse TOT value of the reference energy value, 511keV. As a result, the coarse TOT distribution, obtained when the calibrated filter discriminates the detected gamma events, presents variable energy cuts adapted to the specific channel energy distribution as shown in the coarse TOT distribution of Figure 11. One of the benefits of channel dependent threshold adjustment, consist in the optimum filter thresholds settings which led to the complete filtering of events outside the valid energy range even for the malfunctioning ASICs. Observing the coarse TOT distribution on Figure 11 we can see how is no more possible to identify the problematic ASICs present on the system by inspection of their energy spaces. Now the filtering process is optimum, for every channel, the DAQ front-end modules only retransmit the gamma events whose energy lays within the specified energy window.

Under these conditions we performed a threshold sweep analysis to find the best energy threshold value for the current system while studying the effect on the data rate reduction. The evolution curve depicted on Figure 12 shows the progression of the data reduction as we increase the lower threshold. We can notice the higher concentration of events with low energy given the tendency of the curve

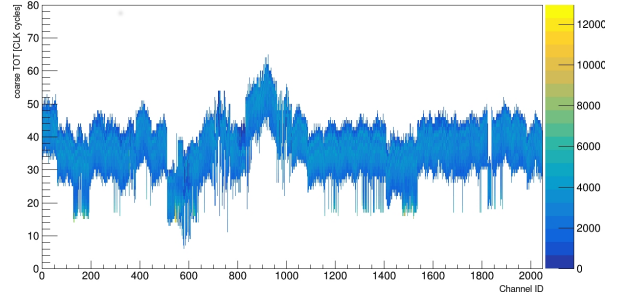


Figure 11: Coarse TOT distribution of the received ASICs events for the 2048 system channels expressed in CLK cycles, 6.25ns. The produced events are the result of a 5min acquisition placing a Na22 point source centered on the detector ring when the DAQ front-end modules implement the calibrated filter.

where for the first values of the threshold the reduction is bigger. This result is in agreement with the energy distribution shown in the coarse TOT distribution of Figure 1. The detailed view of the region of interest in the right side plot of the figure shows how the lower energy range concentrates the biggest amount of events. Once the low threshold surpasses 150keV the evolution on the rate reduction is not so steep. System simulations indicate how the low energy cut value which finds the best compromise between system's sensitivity and data output rate is 225keV for the EndoTOFPET-US system[13]. When we set a lower filter threshold equal to 225keV we obtained a 80% data rate reduction as shown in the evolution curve depicted on Figure 12.

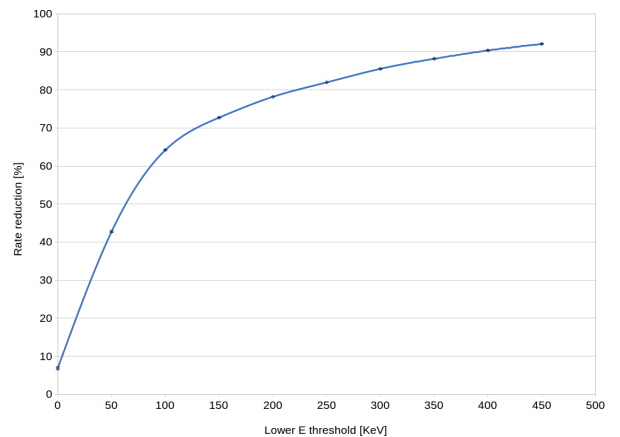


Figure 12: Rate reduction obtained through the increment of the low filter threshold when the DAQ front-end modules implement the calibrated filter. We express the rate reduction as the percentage relative to the reference non filtering case.

To analyze the complexity of the calibrated filter version we studied the resources it needs when we implement it on the target FPGA. The FPGA utilization report shows us how there is not a big increment in the resources demand of this version in comparison with the uncalibrated one. The calibrated filter consumes in total for the implementation of the filtering module plus the changes on the configuration module the following FPGA resources for the device under use, Xilinx Kintex7 XC7K160T:

- 292 slice LUTs, 0.29% of the total number of slice LUTs in the device.
- 538 slice registers, 0.27% of the total number of slice registers in the device.
- 133 slices, 0.52% of the total number of slices in the device.

This is a negligible increment on the resources needs in comparison with the uncalibrated filter version. The significant resources consumption difference between both filter versions comes from the implementation of the LUT to store the filtering thresholds of every channel. The implementation of this memory block consumes one FPGA block RAM tile, which represent 0.31% of all the FPGA block RAM tiles on the device under use, Xilinx Kintex7 XC7K160T.

Under the light of these results, we see how the volume of data is effectively reduced by the filter which clears out exclusively those events laying outside the valid energy range. Despite the indications of proper energy discrimination shown on the coarse TOT distribution of Figure 12, we need to prove that the usage of the on-line energy filter does not alter the performance of the system. To ensure that the filtering process is transparent to the system performance, we compared the resulting energy and time resolutions of the system in the cases of using or excluding the filter. The energy spectrum comparison of Figure 13 shows the original energy spectrum of the unfiltered data in red color and the filtered case in blue. For this experiment we set a 150keV low threshold and 900keV on the upper one. Observing the energy spectrum obtained through the filter on Figure 12, we can check how this thresholds are properly set because the filter lets pass only those events whose energy lies within these two values. The accuracy setting the filter thresholds is merely determined by the accuracy on

the energy calibration process. For those systems whose calibration process place the optimization focus on a small energy range close to the 511keV photo-peak, only thresholds set on a range around this value will be accurate. In this case, the further apart the thresholds are from the photo-peak, the poorer its accuracy will be. Given the fact that the relationship between coarse TOT and energy is exponential, the resolution is better for the lower energies than for the higher ones. Studying the energy spectrum comparison we can conclude that, when the DAQ front-end modules include the filter, it preserves its original energy resolution because the energy distribution in the photo-peak is the same for both cases, i.e. we get the same Gaussian fit curve for both energy spectrums.

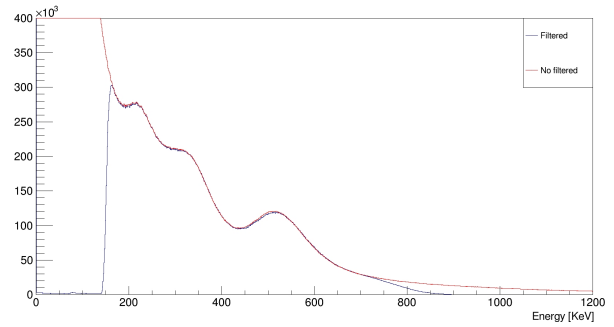


Figure 13: Energy spectrums produced by the received ASICs events. The received events are the result of a 5min acquisition placing a Na22 point source centered on the detector when the DAQ implements no filtering at all, red curve, or when the DAQ front-end modules apply the calibrated energy filter, blue curve.

We have demonstrated how the filter does not disturb the system's energy resolution but we still need to prove that the system maintains its temporal properties as well. For this purpose, we perform a comparison of the obtained Coincidence Time Resolution (CTR) distributions. The CTR distribution on the upper plot of Figure 14 shows the CTR distribution of the system when the DAQ implements no filtering and the lower plot displays the resulting distribution when the DAQ front-end modules apply the calibrated filter setting its lower and upper thresholds to 150keV and 900keV respectively. The timing results shown in Figure 14 prove the preservation of the timing properties of the system during the filtering process. For both cases, most of the recorded Lines-Of-Response (LOR) present CTR values around 800ps Full Width Half Maximum (FWHM). This is a poor time resolution

for a TOF PET system and is not in agreement with the previous time resolution reported for this system[11]. The reason for having a different time resolution in this experiment is the need to deactivate the software post-processing which corrects the events time stamps off-line. Only making use of this post-processing correction the system may achieve the average CTR values of 375ps FWHM.

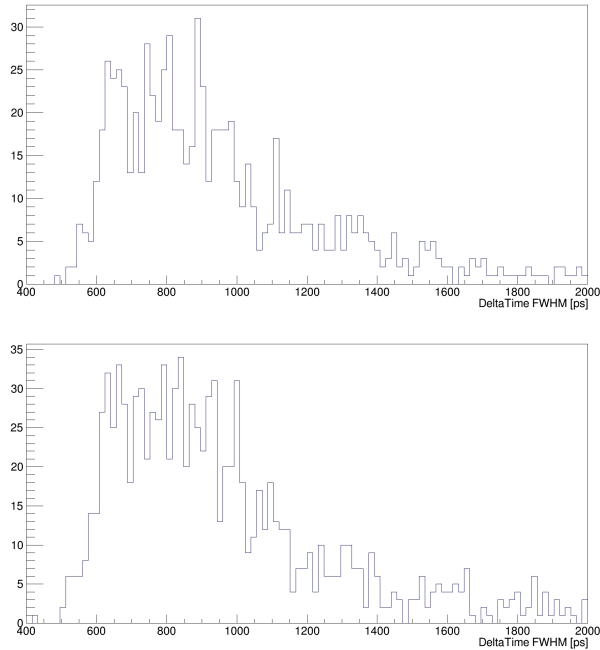


Figure 14: CTR distributions produced by the received ASICs events. The received events are the result of a 5min acquisition placing a Na22 point source centered on the detector when the DAQ implements no filtering at all, upper graph. And when the DAQ front-end modules apply the calibrated energy filter, lower plot.

The ASIC measures the time of arrival of events reading the charge deposited in a capacitor. Due to a problem on the TOFPET ASIC design, this capacitor leakages and thus the charge read from the capacitor does not corresponds to the charge associated with its time of arrival. PETsys characterized this leakage, thus knowing the time between consecutive events, the post-processing script can compensate the charge read from the leaking capacitor. Consequently, on systems making use of the TOFPET ASIC, the post-processing script needs the time information of the precedent event to correct the time stamp of the valid current gamma event independently of the validity of the previous event. As a result, when the DAQ filters out a

non valid event, the system loses the correction information needed for the following event. Given this particularity of the TOFPET ASIC, the on-line energy filter will only preserve the time properties of the system before applying the software post-processing time correction.

4. Discussion

Under the light of the results exposed in the results Section 3, we have seen how the proposed implementations of the on-line energy filters are effective solutions for the reduction of the data rate in highly pixelated TOF PET systems with digital readout while preserving the system performance in terms of sensitivity and resolution (energy and time). This is a lightweight solution capable of setting an energy acceptance window on demand to ease the system BW requirements. This technique proves to be specially useful for systems that include malfunctioning ASICs, which is common on highly pixelated systems comprising tens of these readout chips. For the exposed case of usage on the PETsys demonstrator, we have seen how these problematic ASICs on the system produce events over the whole energy range. Using the on-line energy filter will contribute to the solution of the BW issue by filtering the events of those ASICs presenting a non valid energy value. Experimental results demonstrate that, for the TOFPET ASIC, the biggest contribution to the data rate reduction comes from the filtering process of the events in the lowest energy range. The coarse TOT distribution on Figure 1 illustrates the higher concentration of low energy events and the coarse TOT histogram of Figure 4 confirms that there are five times more events in the lowest energy range than in the range of interest. TOFPET ASIC fails to achieve proper adjustment of its triggering scheme and thus it triggers on the reception of any detected pulse, even those with the lowest energies. Hence we can conclude that the ASIC is triggering on noise. Non being able to correct this behavior for the current readout chip, the system collects more non-valid events than valid ones. On this system, when the DAQ front-end modules implement an on-line calibrated filtering stage and setting a low threshold on 225keV we achieve an 80% data reduction. An energy cut on 225keV has proven on simulations to be the optimum limit to reduce the percentage of non-valid events while preserving system sensitivity[13]. As a consequence, we can conclude that the current

system presents a poor signal to noise ratio, around 1:4, and thus it could highly benefit from an on-line filtering to remove the ASICs events produced from noise. In general, systems producing non valid events along with real gamma photon events find on the on-line energy filter a good solution for the efficient reduction of the system's output data rate.

Despite the proved efficiency of the filter, we have identified a couple of unexpected discrepancies on the system behavior that alter the filter outcome:

- TOFPET ASIC interdependence between consecutive events. The system needs to compensate the time information of the current event using the information of the precedent one. As a consequence, the DAQ associated to the TOFPET ASIC should not apply the on-line energy filtering to preserve the system's time resolution. Although systems readout by TOFPET ASIC chips should not apply this technique because of this ASIC particularity, we have been able to prove on this system the efficiency of the filtering process by deactivating the SW post-processing dealing with the compensation of the corrupted timestamps. When we disable this process, we observe how the time resolution does not vary when the DAQ implements the filter.
- High sensitivity to the energy calibration accuracy and temperature variations. By definition, the calibrated filter implementation is highly dependent on the energy calibration information. This calibration process is not straight forward in systems with thousands of channels. The curve fitting algorithm on search of the optimum TOT-energy curve does not always converge for all the system channels. For these non converging channels we have set the energy relationship found on the previous channel which exhibits a valid energy curve fit. Furthermore, given the strong exponential TOT-energy relationship, the energy calibration for the higher energy values is not so accurate as for the energies in the region of interest. Given these unexpected issues on the energy calibration process and the strong dependence of the filter to the calibration information, we found that a poor energy calibration will lead to an inaccurate positioning of the filter thresholds. Furthermore, SiPMs are highly sensitive to temperature variations[14] and changes in temperature will lead to a

change on the TOT-energy relationship. Temperature variations make the present energy calibration information not valid for the new system conditions and thus the filter will fail to accurately define its filtering limits.

Comparing the similar resources consumption and the rate reduction results obtained for the uncalibrated and the calibrated filter implementations we deduce that, in general, the calibrated filter version gives a better noise reduction on pixelated PET systems than its uncalibrated counterpart. However, given the good rate reduction results obtained using the uncalibrated filter implementation, we conclude that the uncalibrated filter version is a good solution for systems with poor or none energy calibration information.

Even-though current results deactivating the post-processing time correction are conclusive enough to prove the efficiency of the on-line filtering technique, we intend to pursue a new test using this technique on a similar system, a highly pixelated PET scanner with digital readout but this time not read by the TOFPET ASIC but a different ASIC. One of the identified tasks as future work is the testing of the on-line energy filter on the second version of the EndoTOFPET-US plate which makes use of the STiC ASIC. The STiC ASIC does not present any interdependence between consecutive events.

Given the strong dependence of the filter with the energy calibration, which is commonly inaccurate for values not close to the photo-peak, and the variability of the system response with temperature changes, we envisaged a new calibration independent filter implementation. This version would read all incoming data, implement a peak-finder algorithm to identify the position (TOT value) of the photo-peak for every channel and we would set the two filtering limits equally spaced on both sides of the photo-peak. This implementation will no more let the user specify the filtering energy limits in keV but instead as a margin around the photo-peak. This margin setting would enable the control of the systems output data volume while maintaining the system performance if the margin is properly set.

Another upgrade conceived for future work consists in the actual correction of the gamma events time stamps for the case of the events undergoing the counter rollover effect. The DAQ front-end modules already process the gamma events time information without modifying it. Correcting these

time stamps would be a straight forward process for the DAQ and thus implementation of such process would add minimal resources needs to the filter. Making use if such on-line processing procedure would exclude the necessity of using an off-line SW preprocessing mechanism to correct the counter rollover events.

Different PET systems found in literature apply on-line data filtering techniques demonstrating its efficiency to reduce the volume of produced data minimizing the presence of non useful information[3][4]. However, this is to our knowledge the first time to apply this kind of techniques on pixelated PET systems with a SiPM-ASIC readout scheme. Pixelated PET systems with a big density of digital channels are prone to present noisy channels. The more noisy channels are present on the system the less BW is available to transmit useful data. Given the ease of access to the digital information of each event on the DAQ front-end level of PET systems with SiPM-ASIC readout, we confirm that energy based event discrimination is a suitable technique to come up with the BW limitation issue present in system with a high count rate as is the case of highly pixelated PET systems.

5. Conclusion

Current trends in PET systems show an increasing interest on highly pixelated systems due to their capability to achieve better spatial resolution than monolithic PET systems. But pixelated detectors increase the complexity of the DAQ system reading out these detectors: a high density of detecting channels produces a high count rate which could reach the system BW limit putting the system into saturation and thus losing valuable information. This work demonstrates how on-line event discrimination based on energy at the front-end level is an efficient and lightweight technique to cope with the BW limitation problem present in highly pixelated PET systems. Furthermore, through this study we have seen how a PET system readout by the TOFPET ASICv1 would profit from the filtering of the non-valid energy events that the ASIC produces for some miss-behaving channels or even for all channels in the case of malfunctioning ASICs. Apart from those scattered non-useful events, this ASIC produces the highest concentration of events is in the lowest energy range. In general, any SiPM-ASIC readout scheme generating events with energies out of the range of interest would reduce its

BW needs making use of an on-line filtering stage discarding those events on the fly. Nonetheless, our analysis also brought into light the timing information corruption issue present on the TOFPET ASICv1 which creates an unexpected interdependence between consecutive events. Due to this particularity of the chip, we concluded that the DAQ front-end modules should not make use this discriminating technique on systems readout by the TOFPET ASICv1. As a consequence, we plan new experiments to test the preference of the on-line energy filter on similar systems readout by other ASICs. Given the results showing the preservation of the system time and energy resolutions, even using the TOFPET ASICv1 when we disable the time correction post-processing mechanism, we conclude that on-line energy filtering is an effective technique for pixelated PET system.

Under a more global scope, this work highlights the potential of applying on-line processing techniques on the DAQ level for pixelated PET systems making use of readout ASICs. Having in hand the digital event information on the DAQ front-end modules, we could apply simple discrimination techniques as the ones here analyzed or more complex implementations as the proposed peak-finder discriminator to get a calibration independent solution.

6. Acknowledgment

This work, as part of PicoSEC MCNet Project, is supported by a Marie Curie Early Initial Training Network Fellowship of the European Communitys Seventh Framework Program [contract number PITN-GA-2011-289355-PicoSEC-MCNet]. And EndoTOFPETUS has received funding from the European Union 7th Framework Program,FP7/2007-2013, [Grant Agreement. No. 256984].

It does exist a potential conflict of interest given the fact that the following co-authors are employees of PETsys Electronics SA: L. Ferramacho, R. Bugalho, C. Leong, T. Niknejad, J. C. Silva, M. Silveira, S. Tavernier, J. Varela. This relationship with the company commercializing one of the devices under study does not incur in any real conflict of interest. We ensure that the information disclosed on this study is completely unbiased and objective.

References

References

- [1] J. R. Stickel, S. R. Cherry, High-resolution PET detector design: modelling components of intrinsic spatial resolution, *Physics in Medicine & Biology* 50 (2) (2005) 179.
URL <http://stacks.iop.org/0031-9155/50/i=2/a=001>
- [2] C. Ritzer, P. Hallen, D. Schug, V. Schulz, Intercrystal Scatter Rejection for Pixelated PET Detectors, *IEEE Transactions on Radiation and Plasma Medical Sciences* 1 (2) (2017) 191–200. doi:10.1109/TNS.2017.2664921.
- [3] X. Wu, J. Zhu, M. Niu, Z. Hu, Q. Xie, P. Xiao, On-line parameter calibration for energy discrimination in trans-PET, *IEEE Nuclear Science Symposium Conference Record* (2013) 3–5doi:10.1109/NSSMIC.2013.6829181.
- [4] P. Conde, A. Iborra, A. J. González, A. Aguilar, E. Díaz-Caballero, J. J. García-Garrigos, A. González-Montoro, D. Grau-Ruiz, S. Sánchez, L. Hernández, P. Bellido, L. Moliner, J. P. Rigla, M. J. Rodríguez-Álvarez, F. Sánchez, M. Seimetz, A. Soriano, L. F. Vidal, J. M. Benlloch, Noise rejection in monolithic PET detectors, in: 2016 IEEE Nuclear Science Symposium, Medical Imaging Conference and Room-Temperature Semiconductor Detector Workshop (NSS/MIC/RTSD), 2016, pp. 1–5. doi:10.1109/NSSMIC.2016.8069574.
- [5] N. Aubry, E. Auffray, F. B. Mimoun, N. Brillouet, R. Bugalho, E. Charbon, O. Charles, D. Cortinovis, P. Courday, a. Cserkaszky, C. Damon, K. Doroud, J. M. Fischer, G. Fornaro, J. M. Fourmigue, B. Frisch, B. Fürst, J. Gardiazabal, K. Gadow, E. Garutti, C. Gaston, a. Gil-Ortiz, E. Guedj, T. Harion, P. Jarron, J. Kabadanian, T. Lasser, R. Laugier, P. Lecoq, D. Lombardo, S. Mandai, E. Mas, T. Meyer, O. Mundler, N. Navab, C. Ortigão, M. Paganoni, D. Perrodin, M. Pizzichemi, J. O. Prior, T. Reichl, M. Reinecke, M. Rolo, H. C. Schultz-Coulon, M. Schwaiger, W. Shen, a. Silenzi, J. C. Silva, R. Silva, I. S. Schweiger, R. Stamen, J. Traub, J. Varela, V. Veckalns, V. Vidal, J. Vishwas, T. Wendler, C. Xu, S. Ziegler, M. Zvolsky, EndoTOFPET-US: a novel multimodal tool for endoscopy and positron emission tomography, *Journal of Instrumentation* 8 (04) (2013) C04002. doi:10.1088/1748-0221/8/04/C04002.
URL <http://stacks.iop.org/1748-0221/8/i=04/a=C04002>
- [6] C. Zorraquino, EndoTOFPET-US a High Resolution Endoscopic PET-US Scanner Used for Pancreatic and Prostatic Clinical Exams, in: L. M. Roa Romero (Ed.), XIII Mediterranean Conference on Medical and Biological Engineering and Computing 2013, Springer International Publishing, Cham, 2014, pp. 451–454.
- [7] B. Frisch, Combining endoscopic ultrasound with Time-Of-Flight PET: The EndoTOFPET-US Project, *Nuclear Instruments and Methods in Physics Research, Section A: Accelerators, Spectrometers, Detectors and Associated Equipment* 732 (2013) 577–580. doi:10.1016/j.nima.2013.05.027.
URL <http://dx.doi.org/10.1016/j.nima.2013.05.027>
- [8] R. Bugalho, C. Gaston, M. D. Rolo, J. C. Silva, R. Silva, J. Varela, EndoTOFPET-US data acquisition system, *Journal of Instrumentation* 8 (02) (2013) C02049–C02049. doi:10.1088/1748-0221/8/02/C02049.
URL <http://stacks.iop.org/1748-0221/8/i=02/a=C02049?key=crossref.53fa6832c5d9e999944e3bb8145d2cdb>
- [9] C. Zorraquino, R. Bugalho, M. Rolo, J. C. Silva, V. Vecklans, R. Silva, C. Ortigão, J. A. Neves, S. Tavernier, P. Guerra, A. Santos, J. Varela, Asymmetric Data Acquisition System for an Endoscopic PET-US Detector, *IEEE Transactions on Nuclear Science* 63 (1) (2016) 213–221. doi:10.1109/TNS.2016.2514600.
- [10] M. D. Rolo, R. Bugalho, F. Gonçalves, G. Mazza, A. Rivetti, J. C. Silva, R. Silva, J. Varela, TOFPET ASIC for PET applications, *Journal of Instrumentation* 8 (02) (2013) C02050.
URL <http://stacks.iop.org/1748-0221/8/i=02/a=C02050>
- [11] T. Niknejad, S. Setayeshi, S. Tavernier, R. Bugalho, L. Ferramacho, A. D. Francesco, C. Leong, M. D. Rolo, M. Shamshirsaz, J. C. Silva, R. Silva, M. Silveira, C. Zorraquino, J. Varela, Validation of a highly integrated SiPM readout system with a TOF-PET demonstrator, *Journal of Instrumentation* 11 (12) (2016) P12003.
URL <http://stacks.iop.org/1748-0221/11/i=12/a=P12003>
- [12] T. Orita, H. Takahashi, K. Shimazoe, T. Fujiwara, S. Boxuan, A new pulse width signal processing with delay-line and non-linear circuit (for ToT), *Nuclear Instruments and Methods in Physics Research Section A: Accelerators, Spectrometers, Detectors and Associated Equipment* 648 (2011) S24 – S27. doi:https://doi.org/10.1016/j.nima.2011.01.023.
URL <http://www.sciencedirect.com/science/article/pii/S0168900211000738>
- [13] M. Zvolsky, Simulation, Image Reconstruction and SiPM Characterisation for a Novel Endoscopic Positron Emission Tomography Detector, Dissertation, Universität Hamburg, Hamburg, dissertation, Universität Hamburg, 2017 (2017). doi:10.3204/PUBDB-2017-13685.
URL <https://bib-pubdb1.desy.de/record/398074>
- [14] M. Ramilli, Characterization of sipm: Temperature dependencies, in: 2008 IEEE Nuclear Science Symposium Conference Record, 2008, pp. 2467–2470. doi:10.1109/NSSMIC.2008.4774854.